

This is the accepted manuscript made available via CHORUS. The article has been published as:

Interface-induced spin-orbit interaction in silicon quantum dots and prospects for scalability

Rifat Ferdous, Kok W. Chan, Menno Veldhorst, J. C. C. Hwang, C. H. Yang, Harshad Sahasrabudhe, Gerhard Klimeck, Andrea Morello, Andrew S. Dzurak, and Rajib Rahman

Phys. Rev. B **97**, 241401 — Published 4 June 2018

DOI: [10.1103/PhysRevB.97.241401](https://doi.org/10.1103/PhysRevB.97.241401)

Interface induced spin-orbit interaction in silicon quantum dots and prospects for scalability

Rifat Ferdous,^{1,*} Kok W. Chan,^{2,†} Menno Veldhorst,³ J.C.C. Hwang,² C. H. Yang,² Harshad Sahasrabudhe,¹ Gerhard Klimeck,¹ Andrea Morello,² Andrew S. Dzurak,² and Rajib Rahman¹

¹*Network for Computational Nanotechnology, Purdue University, West Lafayette, IN 47907, USA*

²*Centre for Quantum Computation and Communication Technology,
School of Electrical Engineering and Telecommunications,*

The University of New South Wales, Sydney, New South Wales 2052, Australia

³*QuTech and Kavli Institute of Nanoscience, TU Delft, Lorentzweg 1, 2628CJ Delft, the Netherlands*
(Dated: May 16, 2018)

We identify the presence of monoatomic steps at the Si/SiGe or Si/SiO₂ interface as a dominant source of variations in the dephasing time of Silicon (Si) quantum dot (QD) spin qubits. First, using atomistic tight-binding calculations we show that the g -factors and their Stark shifts undergo variations due to these steps. We compare our theoretical predictions with experiments on QDs at a Si/SiO₂ interface, in which we observe significant differences in Stark shifts between QDs in two different samples. We also experimentally observe variations in the g -factors of one-electron and three-electron spin qubits realized in three neighboring QDs on the same sample, at a level consistent with our calculations. The dephasing times of these qubits also vary, most likely due to their varying sensitivity to charge noise, resulting from different interface conditions. More importantly, from our calculations we show that by employing the anisotropic nature of the spin-orbit interaction (SOI) in a Si QD, we can minimize and control these variations. Ultimately, we predict that the dephasing times of the Si QD spin qubits will be anisotropic and can be improved by at least an order of magnitude, by aligning the external DC magnetic field towards specific crystal directions, given other decoherence mechanisms do not dominate over charge noise.

A scalable quantum computing architecture requires reproducibility and control over key qubit properties, such as resonance frequency, coherence time, etc. Variability in such parameters among qubits of a large-scale quantum computer would necessitate individual qubit characterization and control¹, while excessive variability could even make scaling impractical. In case of significant variability in the dephasing time, the qubit that decoheres the fastest might limit the overall performance.

Spin qubits hosted in Si QDs² have been showing promise as a potential building block for a large-scale quantum computer³, because of their compatibility with already existing CMOS technology and the long coherence times available due to the presence of negligible nuclear spins in isotopically purified ²⁸Si⁴. Single^{5–10} and two qubit¹¹ gates have been demonstrated already. To move forward with increasing numbers of qubits^{1,12–14}, we have to study possible sources that can cause variations in the coherence time and limit the performance of these qubits.

In this letter, we provide a microscopic understanding of the dephasing time T_2^* of Si QD spin qubits. We show that electrical noise modulates the electron g -factor through SOI and causes dephasing. Moreover, the atomic scale details of the interface controls the sensitivity of the g -factor to the electric field or noise and hence introduce variability in the T_2^* times. We experimentally observe variations in the g -factors, their gate voltage dependence and T_2^* times among spin qubits hosted in gate-defined quantum dots formed at a Si/SiO₂ interface. Finally we predict that, due to the anisotropic nature of the SOI in Si QDs, the T_2^* times will be anisotropic and hence

can be improved and their variability can be reduced as well by choosing the appropriate direction of the external magnetic field.

The energy levels of interest in a Si QD for qubit operations are two low lying conduction band valley states v_- and v_+ , each split in two spin levels in the presence of a DC magnetic field, B_{ext} . All subsequent symbols with subscript $-$ ($+$) corresponds to the v_- (v_+) valley state. However, it turns out that the spin splitting ($E_{\text{ZS}}^{\pm} = g_{\pm}\mu_B B_{\text{ext}}$, where μ_B is the Bohr magneton) and also the dephasing time T_2^* are valley dependent^{9,15–18} and, as we will show experimentally, is sample-to-sample dependent.

In a Si quantum well or dot, the presence of structure inversion asymmetry introduces the Rashba SOI^{19–21}. Though it is known that due to the lack of bulk inversion asymmetry, the Dresselhaus SOI is absent from bulk Si, interface inversion asymmetry contributes a Dresselhaus-like term in interface confined structures in Si^{19–21}. Both the Rashba and Dresselhaus SOI modify the electron g -factors in a Si QD, and enable the Stark shift of the g -factors through gate voltage tuning^{8,15,22}. The different sign of the Rashba (α_{\pm}) and Dresselhaus coefficients (β_{\pm}) results in different g -factors among the two valley states¹⁵. The Dresselhaus contribution is usually much stronger than the Rashba SOI^{18,21}, and dominates the g -factor renormalization¹⁸. These SOI effects also make the qubits susceptible to electrical noise.

In a Si QD with a strong vertical electric field, the electrons are usually confined to only one interface. A monoatomic shift in the location of this interface results in a sign inversion of the Dresselhaus coefficient, while the

Rashba coefficient remains unchanged^{19–21}. In practice, Si/SiGe or Si/SiO₂ interfaces certainly contain roughness, i.e. monoatomic steps^{23–25}. A non-ideal interface with monoatomic steps can be thought of as multiple smooth interface regions, where interfaces of neighboring regions are shifted by one atomic layer with respect to each other. Thus the neighboring regions will have opposite signs of β . An electron wavefunction spread over multiple such regions will witness multiple local β s and the effective β will be a weighted average. Thus the presence of interface steps can change both the sign and magnitude of the effective Dresselhaus contribution to the electron g -factors in a Si QD¹⁸. In essence, local changes in the orientation of chemical bonds of the atoms at the interface inside a dot may result in similar effects. To accurately understand these atomic-scale physics of the interface, here we use spin resolved $sp^3d^5s^*$ tight-binding model, where the effects of the SOI comes out automatically based on the atomic arrangement of the QD, without any pre-assumption about the Rashba or Dresselhaus SOI.

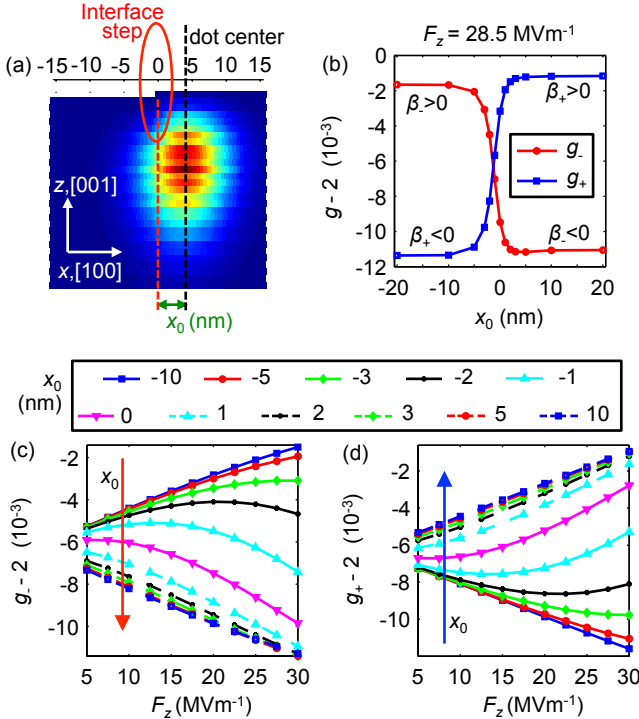


FIG. 1. Effect of interface steps on g -factors and their Stark shifts in a Si QD from atomistic tight-binding calculation. (a) An electron wavefunction subject to an interface step. (b) Variation in the g -factors for both valley states (g_- and g_+), as a function of x_0 for vertical electric field $F_z = 28.5 \text{ MVm}^{-1}$. When the electron is on the left (right) side of the step, β_- is positive (negative) and β_+ is negative (positive) and we see, $g_- > g_+$ ($g_- < g_+$). F_z dependence of (c) g_- and (d) g_+ for various x_0 . The magnetic field used in the simulations of Figs. 1b, 1c and 1d is 1.4 T along the [110] crystal orientation and the monoatomic step is parallel to the y ([010]) direction.

Fig. 1 shows how a monoatomic step at the interface of a Si QD can affect the g -factors of the valley states and their electric field dependence, with an external magnetic field along the [110] crystal orientation, from atomistic tight-binding simulations. The distance between the dot center and the location of the edge of the interface step is denoted by x_0 (shown in Fig. 1a). The dot radius is around 10 nm. So for $x_0 < -10 \text{ nm}$ the dot is completely on the left side of the step and has different g -factors ($g_- > g_+$) compared to that ($g_+ > g_-$) for $x_0 > 10 \text{ nm}$, when the dot is completely on the right side of the step, as seen in Fig. 1b. For $-10 \text{ nm} < x_0 < 10 \text{ nm}$, the g -factors are a weighted average of those of the two sides based on the dot location. To understand this atomistic calculation we use an analytic effective mass model that relates g_{\pm} in a Si QD, with the Rashba and Dresselhaus SOI^{15,18}. We briefly summarize this model in the Supplemental Material²⁶. For B_{ext} along the [110] crystal orientation

$$\delta g_{\pm}^{[110]} = g_{\pm}^{[110]} - g_{\perp} = 2 \frac{|e| \langle z \rangle}{\mu_B \hbar} (-\alpha_{\pm} + \beta_{\pm}) \quad (1)$$

Here, $g_{\perp} = 1.9937$ is the g -factor perpendicular to the valley axis^{18,27}, $|e|$ is the electron charge, $\langle z \rangle$ is the spread of the electron wavefunction along the vertical direction z ([001]) and \hbar is the reduced Planck constant. Now, in a Si QD, $\beta \gg \alpha^{18,21}$, and so

$$\delta g_{\pm}^{[110]} \approx 2 \frac{|e| \langle z \rangle}{\mu_B \hbar} \beta_{\pm} \quad (2)$$

As previously discussed, β has a different sign between the two sides of the step. When the location of the dot changes with respect to the step, the weighted average of the positive and negative β s change, which changes the g -factors.

Figs. 1c and 1d show that the Stark shift of the g -factors, as a function of the confining vertical electric field F_z , for both valley states are also affected by the presence of an interface step. The differential change in the g -factors with electric field, $\frac{dg_{\pm}}{dF_z}$, can vary in both sign and magnitude depending on the location of the step. This behavior can also be explained by equation 2, with the change in β near an interface step. For example in Fig. 1c, for $x_0 \approx -10 \text{ nm}$, the dot is completely on the left side of the step, where the v_- valley state has positive β . Thus an increase in β_- with increasing F_z increases g_- as well, hence a positive $\frac{dg_-}{dF_z}$. On the other hand, when the dot is completely on the right side of the step, at $x_0 \approx 10 \text{ nm}$, β_- is negative. Thus increasing F_z increases $|\beta_-|$ but decreases g_- and thus results in a negative $\frac{dg_-}{dF_z}$. For $-10 \text{ nm} < x_0 < 10 \text{ nm}$, $\frac{dg_-}{dF_z}$ changes gradually with x_0 . We see a similar but opposite change for g_+ in Fig. 1d.

Similar variations in the g -factors, and their gate voltage dependence, are measured in gate-defined quantum dots formed at a Si/SiO₂ interface for two different samples (A and B) with similar architecture. Fig. 2b shows variations in one-electron and three-electron g -factors

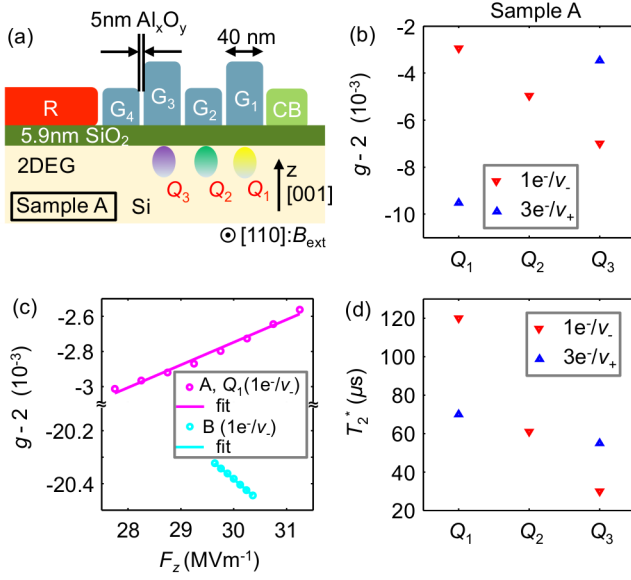


FIG. 2. Schematic diagram of the experimental sample and observed dot-to-dot variations. (a) Cross sectional schematic of sample A. CB acts as a lateral confinement gate in the formation of quantum dots under gates G_1 , G_2 , and G_3 . G_4 is used as a tunnel barrier for loading/unloading of electrons from the 2DEG formed under the reservoir (R) gate. The external magnetic field is applied along the $[110]$ crystal orientation, which is going out of the plane of the paper. (b) Variation in the g -factors, both one-electron (g_-) and three-electron (g_+), among three neighboring quantum dots (Q_1 , Q_2 , Q_3) formed at the Si/SiO₂ interface in sample A. (c) One-electron Stark shift of Q_1 from sample A and one QD from sample B plotted together as a function of the vertical electric field, F_z . Note that both samples were measured in different dilution fridges and there is an unknown B_{ext} offset in sample B, contributing to larger discrepancy in its g -factor from 2. (d) Observed variations in the dephasing times among qubits in sample A.

among Q_1 , Q_2 and Q_3 , in sample A (schematic shown in Fig. 2a). We understand that the one-electron (three-electron) qubit corresponds to an electron occupying the lower (higher) energy valley state v_- (v_+)¹⁵. We could not achieve three-electron spin resonance for Q_2 as it was strongly coupled to the other dots. In Fig. 2c we see that the g_- of Q_1 has opposite dependence on F_z compared to that of the one QD in sample B. These observed variations in both the Stark shifts and the g -factors qualitatively agree with the theoretically predicted variations shown in Fig. 1. We therefore conclude that these experimentally observed variations are primarily due to different interface conditions associated with each of the QDs.

We also observe variations in the measured T_2^* times, extracted by performing Ramsey experiments²⁶, for both valley states of the three QDs in sample A, as shown in Fig. 2d.

The dephasing time due to nuclear spin fluctuations is given in refs.^{28,29} and in our samples, which employ an

isotopically enriched ^{28}Si substrate, these times are very long. In the absence of nuclear spin, we can relate T_2^* times with electrical noise in a similar way,

$$T_2^* = \frac{\sqrt{2}\hbar}{\sum_{i=x,y,z} \Delta F_i \left| \frac{dg}{dF_i} \right| \mu_B B_{\text{ext}}} \quad (3)$$

Here, ΔF_i is the standard deviation of the electric field fluctuation seen by the dot, due to electrical noise on the gate. As all of the dots are formed directly underneath the gates, any fluctuation in the top gate (e.g. fluctuation in G_1 for Q_1) will dominate the total field fluctuation. A fluctuation in the top gate will cause $\Delta F_z \gg \Delta F_{x/y}$. From our Sentaurus TCAD simulations²⁶ we find that, $\frac{\Delta F_z}{\Delta V_{g_1}^{\text{top}}} = -5.34 \mu\text{m}^{-1}$ and $\frac{\Delta F_x}{\Delta V_{g_1}^{\text{top}}} = 0.2 \mu\text{m}^{-1}$, whereas $\frac{\Delta F_z}{\Delta V_{g_1}^{\text{side}}} = -3.52 \mu\text{m}^{-1}$ and $\frac{\Delta F_x}{\Delta V_{g_1}^{\text{side}}} = -1.52 \mu\text{m}^{-1}$ for 5 nm gate separation (Fig. 2a). Here $\Delta V_{g_1}^{\text{top}}$ ($\Delta V_{g_1}^{\text{side}}$) is a voltage fluctuation in the top (side) gate. Larger gate separation will reduce $\frac{\Delta F_{x/y/z}}{\Delta V_{g_1}}$.

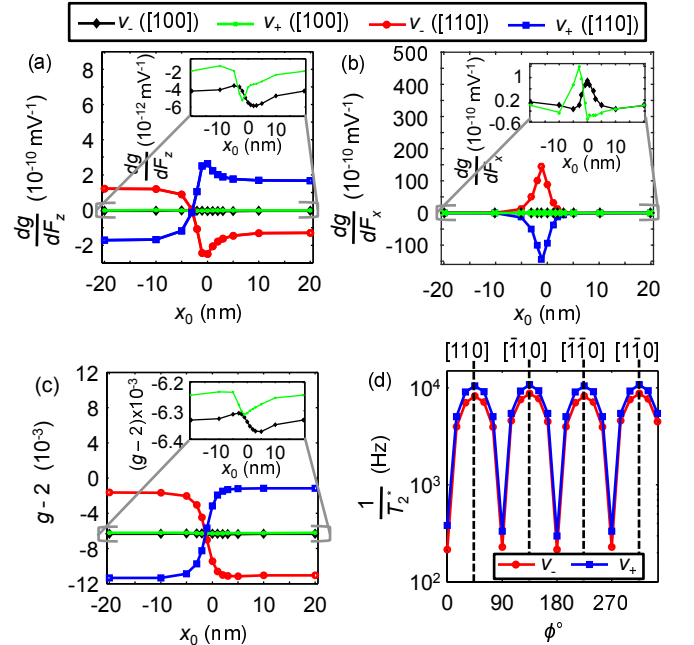


FIG. 3. Change in (a) $\frac{dg_{\pm}}{dF_z}$, (b) $\frac{dg_{\pm}}{dF_x}$ and (c) g_{\pm} as a function of x_0 with B_{ext} along $[110]$ and $[100]$ (inset), for $F_z = 28.5 \text{ MVm}^{-1}$, calculated using atomistic tight-binding model. (d) $\frac{1}{T_2^*} = \frac{1}{T_2^*(\Delta F_z)} + \frac{1}{T_2^*(\Delta F_x)}$ with respect to the direction of B_{ext} , ϕ , for $x_0 = -6 \text{ nm}$, $F_z = 28.5 \text{ MVm}^{-1}$ and $B_{\text{ext}} = 1.4015 \text{ T}$. T_2^* is calculated using equation 3 for $\Delta F_z = 400 \text{ Vm}^{-1}$ and $\Delta F_x = 80 \text{ Vm}^{-1}$, with $\frac{dg_{\pm}}{dF_z}$ and $\frac{dg_{\pm}}{dF_x}$ calculated from atomistic simulations.

The observed variations in T_2^* can be explained from the changes in $\frac{dg_{\pm}}{dF_z}$ and $\frac{dg_{\pm}}{dF_x}$ with interface step location, as shown in Figs. 3a and 3b. When we compare the T_2^* times between the two valley states of Q_1 , we see

$T_2^*(v_-, Q_1) \approx 1.7 T_2^*(v_+, Q_1)$ and from ref.¹⁵ we find, $\left| \frac{dg_{\pm}^{Q_1}}{dF_z} \right| \approx 2.2 \left| \frac{dg_{\pm}^{Q_1}}{dF_z} \right|$. This almost linear dependence of $\frac{1}{T_2^*}$ on $\left| \frac{dg_{\pm}}{dF_z} \right|$ shows the dominating contribution of ΔF_z on T_2^* for Q_1 . However, comparing Fig. 3a and 3b we see that, $\left| \frac{dg_{\pm}}{dF_x} \right|$ can be larger than $\left| \frac{dg_{\pm}}{dF_z} \right|$ depending on the interface condition. In presence of steps and SOI, the up and down spin wavefunctions move away from each other. For steps parallel to the y direction, $\langle \downarrow | x | \downarrow \rangle \neq \langle \uparrow | x | \uparrow \rangle$, and hence $\left| \frac{dg_{\pm}}{dF_x} \right|$ becomes nonzero. Further details about $\frac{dg_{\pm}}{dF_{x/y}}$ are presented in the Supplemental Material²⁶.

The calculations of Figs. 1 and 3 and the experimental observations of Fig. 2 highlight the device-to-device variability issues that would require individual knowledge of each qubit, and impose a challenge to the implementation of a large scale quantum computer. Any possible way of reducing the variability is crucial to the scale up of Si QD spin qubits. Also an increase in T_2^* , regardless of the interface condition, will aid scalability. Next we investigate ways to improve these issues.

One obvious way to suppress these variabilities is to minimize interface roughness, which is a well known fabrication challenge. Here we propose an alternate approach. As predicted in ref.¹⁸, the g -factors in a Si QD are anisotropic. We can study the anisotropy from a simplified expression^{18,26},

$$\delta g_{\pm} \approx 2 \frac{|e| \langle z \rangle}{\mu_B \hbar} (-\alpha_{\pm} + \beta_{\pm} \sin 2\phi) \quad (4)$$

Here, ϕ is the angle of B_{ext} with the [100] crystal orientation. From equation 4 we see that the contribution of the Dresselhaus SOI is anisotropic and can be tuned by changing the direction of B_{ext} . For example, when B_{ext} is along [100], $\phi = 0^\circ$ and

$$\delta g_{\pm}^{[100]} \approx -2 \frac{|e| \langle z \rangle}{\mu_B \hbar} \alpha_{\pm} \quad (5)$$

Comparing equation 2 and 5 we see that, $\frac{\delta g_{\pm}^{[100]}}{\delta g_{\pm}^{[110]}} \approx \frac{\alpha_{\pm}}{\beta_{\pm}}$. As the effect of the monoatomic steps is more dramatic on β_{\pm} , the change in g_{\pm} and $\frac{dg_{\pm}}{dF_z}$ with interface steps should be smaller for B_{ext} along [100] compared to that for [110]. Moreover, since $\beta_{\pm} \gg \alpha_{\pm}$ ^{18,21}, $\frac{dg_{\pm}}{dF_z}$ itself will be much smaller for [100].

Fig. 3a also compares variations in $\frac{dg_{\pm}}{dF_z}$ with x_0 between B_{ext} along [110] and [100]. Though there are variations in $\frac{dg_{\pm}}{dF_z}$ with x_0 for B_{ext} along [100], as shown by the inset of Fig. 3a, these variations and also $\frac{dg_{\pm}}{dF_z}$ themselves are negligible, when compared to that along [110]. We see a similar reduction in $\frac{dg_{\pm}}{dF_x}$ (and its variability with x_0) for B_{ext} along [100] in Fig. 3b. Variation of g_{\pm} with x_0 , will also be negligible for B_{ext} along [100]³⁰, as shown

in Fig. 3c. Such phenomena will have a critical impact on the realization of a large scale quantum computer made of Si QDs. If the external magnetic field is along the [100] crystal orientation, all the qubits will have negligible variations in g_{\pm} , $\frac{dg_{\pm}}{dF_z}$, $\frac{dg_{\pm}}{dF_{x/y}}$ and consequently in T_2^* even in the presence of varying interface conditions. Very small $\left| \frac{dg_{\pm}}{dF_z} \right|$ and $\left| \frac{dg_{\pm}}{dF_{x/y}} \right|$ along [100] would also result in very long T_2^* times.

In Fig. 3d, the angular dependence of $\frac{1}{T_2^*} = \frac{1}{T_2^*(\Delta F_z)} + \frac{1}{T_2^*(\Delta F_x)}$ for $x_0 = -6$ nm, is shown. Here $T_2^*(\Delta F_{z/x}) = \frac{\sqrt{2}\hbar}{\Delta F_{z/x} \left| \frac{dg_{\pm}}{dF_{z/x}} \right| \mu_B B_{\text{ext}}}$. As the monoatomic step used in the calculation is parallel to the [010] crystal orientation, $\frac{dg_{\pm}}{dF_y}$ and thus $T_2^*(\Delta F_y)$ is negligible. Similar angular dependence of $\frac{1}{T_2^*}$ for $x_0 = 0$ nm is shown in the Supplemental Material²⁶. We can see here that a large increase in T_2^* (> 1 ms) is achievable by orientating B_{ext} along [100]/[010]/ $\bar{[100]}$ /[0 $\bar{1}$ 0].

Now, a decrease in $\left| \frac{dg_{\pm}}{dF_z} \right|$ would also mean a reduced tunability of the g -factors, which is necessary for selective addressing of individual qubits. However, an increase in T_2^* times will result in a narrower electron spin resonance (ESR) linewidth, $\delta f_{\text{FWHM}} = \frac{2\sqrt{\ln 2}^9}{\pi T_2^*}$, which would then require a smaller difference in g -factors between qubits to individually address them.

Orienting the magnetic field along the [100] crystal orientation results in a Dresselhaus SOI with only off-diagonal components²⁶. Therefore, electric field fluctuations, to first order, contribute to spin dephasing through the weaker Rashba SOI, ensuring a long T_2^* time. At the same time, a resonant oscillating electric field can induce electric dipole spin resonance (EDSR) through the off-diagonal Dresselhaus coupling. Since T_2^* is long under these conditions, coherent operations can be expected even for relatively weak EDSR driving strength, and without invoking the use of micromagnets⁹.

To conclude, the presence of random monoatomic steps at the interface of a Si QD can cause variations in both the sign and magnitude of the Dresselhaus SOI among neighboring Si QDs. As a result, the electron g -factors and their sensitivity to electric field should vary, which also leads to variability in the dephasing times among quantum dot spin qubits in Si. The extent of these variations is such that, g -factors, Stark shifts and dephasing times for v_- valley state can be larger than that of the v_+ valley state for some dots while vice versa for others, even with similar range of vertical electric field across dots. Likewise, the Stark shifts for the same valley state can change sign between dots. We also experimentally observe such variations, consistent with the theoretical understanding. We further show that even in the presence of interface steps we can control and minimize these variations by taking advantage of the anisotropic nature of SOI in a Si QD. Importantly, we can increase T_2^* times if we align the external magnetic field along the [100]

crystal orientation, rather than along [110], which will also help to reduce the SOI induced dephasing in Si QD devices with integrated micro-magnets, as SOI also contributes to the g -factors in these devices¹⁸. These theo-

retical findings will guide future experiments to dig into the variability issues in detail and explore the role of the spin-orbit interaction in Si QDs.

-
- * rferdous@purdue.edu
† kokwai@unsw.edu.au
- ¹ L. M. K. Vandersypen, H. Bluhm, J. S. Clarke, A. S. Dzurak, R. Ishihara, A. Morello, D. J. Reilly, L. R. Schreiber, and M. Veldhorst, (2016), arXiv:1612.05936.
 - ² D. Loss and D. P. DiVincenzo, *Phys. Rev. A* **57**, 120 (1998).
 - ³ F. A. Zwanenburg, A. S. Dzurak, A. Morello, M. Y. Simmons, L. C. L. Hollenberg, G. Klimeck, S. Rogge, S. N. Coppersmith, and M. A. Eriksson, *Rev. Mod. Phys.* **85**, 961 (2013).
 - ⁴ K. M. Itoh and H. Watanabe, *MRS Commun.* **4**, 143 (2014).
 - ⁵ B. M. Maune, M. G. Borselli, B. Huang, T. D. Ladd, P. W. Deelman, K. S. Holabird, A. A. Kiselev, I. Alvarado-Rodriguez, R. S. Ross, A. E. Schmitz, M. Sokolich, C. A. Watson, M. F. Gyure, and A. T. Hunter, *Nature* **481**, 344 (2012).
 - ⁶ D. Kim, Z. Shi, C. B. Simmons, D. R. Ward, J. R. Prance, T. S. Koh, J. K. Gamble, D. E. Savage, M. G. Lagally, M. Friesen, S. N. Coppersmith, and M. A. Eriksson, *Nature* **511**, 70 (2014).
 - ⁷ X. Wu, D. R. Ward, J. R. Prance, D. Kim, J. K. Gamble, R. T. Mohr, Z. Shi, D. E. Savage, M. G. Lagally, M. Friesen, S. N. Coppersmith, and M. A. Eriksson, *Proc. Natl. Acad. Sci. U. S. A.* **111**, 11938 (2014).
 - ⁸ M. Veldhorst, J. C. C. Hwang, C. H. Yang, A. W. Leenstra, B. de Ronde, J. P. Dehollain, J. T. Muhonen, F. E. Hudson, K. M. Itoh, A. Morello, and A. S. Dzurak, *Nat. Nanotechnol.* **9**, 981 (2014).
 - ⁹ E. Kawakami, P. Scarlino, D. R. Ward, F. R. Braakman, D. E. Savage, M. G. Lagally, M. Friesen, S. N. Coppersmith, M. A. Eriksson, and L. M. K. Vandersypen, *Nat. Nanotechnol.* **9**, 666 (2014).
 - ¹⁰ K. Eng, T. D. Ladd, A. Smith, M. G. Borselli, A. A. Kiselev, B. H. Fong, K. S. Holabird, T. M. Hazard, B. Huang, P. W. Deelman, I. Milosavljevic, A. E. Schmitz, R. S. Ross, M. F. Gyure, and A. T. Hunter, *Sci. Adv.* **1** (2015).
 - ¹¹ M. Veldhorst, C. H. Yang, J. C. C. Hwang, W. Huang, J. P. Dehollain, J. T. Muhonen, S. Simmons, A. Laucht, F. E. Hudson, K. M. Itoh, A. Morello, and A. S. Dzurak, *Nature* **526**, 410 (2015).
 - ¹² D. M. Zajac, T. M. Hazard, X. Mi, E. Nielsen, and J. R. Petta, *Phys. Rev. Appl.* **6**, 054013 (2016).
 - ¹³ C. Jones, M. A. Fogarty, A. Morello, M. F. Gyure, A. S. Dzurak, and T. D. Ladd, (2016), arXiv:1608.06335.
 - ¹⁴ M. Veldhorst, H. G. J. Eenink, C. H. Yang, and A. S. Dzurak, *Nat. Commun.* **8**, 1766 (2017).
 - ¹⁵ M. Veldhorst, R. Ruskov, C. H. Yang, J. C. C. Hwang, F. E. Hudson, M. E. Flatté, C. Tahan, K. M. Itoh, A. Morello, and A. S. Dzurak, *Phys. Rev. B* **92**, 201401 (2015).
 - ¹⁶ P. Scarlino, E. Kawakami, D. R. Ward, D. E. Savage, M. G. Lagally, M. Friesen, S. N. Coppersmith, M. A. Eriksson, and L. M. K. Vandersypen, *Phys. Rev. Lett.* **115**, 106802 (2015).
 - ¹⁷ P. Scarlino, E. Kawakami, T. Jullien, D. R. Ward, D. E. Savage, M. G. Lagally, M. Friesen, S. N. Coppersmith, M. A. Eriksson, and L. M. K. Vandersypen, *Phys. Rev. B* **95**, 165429 (2017).
 - ¹⁸ R. Ferdous, E. Kawakami, P. Scarlino, M. P. Nowak, D. R. Ward, D. E. Savage, M. G. Lagally, S. N. Coppersmith, M. Friesen, M. A. Eriksson, L. M. K. Vandersypen, and R. Rahman, (2017), arXiv:1702.06210.
 - ¹⁹ L. E. Golub and E. L. Ivchenko, *Phys. Rev. B* **69**, 115333 (2004).
 - ²⁰ M. O. Nestoklon, L. E. Golub, and E. L. Ivchenko, *Phys. Rev. B* **73**, 235334 (2006).
 - ²¹ M. O. Nestoklon, E. L. Ivchenko, J.-M. Jancu, and P. Voisin, *Phys. Rev. B* **77**, 155328 (2008).
 - ²² C. H. Yang, A. Rossi, R. Ruskov, N. S. Lai, F. A. Mohiyaddin, S. Lee, C. Tahan, G. Klimeck, A. Morello, and A. S. Dzurak, *Nat. Commun.* **4**, 2069 (2013).
 - ²³ H. J. W. Zandvliet and H. B. Elswijk, *Phys. Rev. B* **48**, 14269 (1993).
 - ²⁴ M. Friesen, M. A. Eriksson, and S. N. Coppersmith, *Appl. Phys. Lett.* **89**, 202106 (2006).
 - ²⁵ N. Kharche, M. Prada, T. B. Boykin, and G. Klimeck, *Appl. Phys. Lett.* **90**, 092109 (2007).
 - ²⁶ See Supplemental Material for details about the analytic model, Ramsey experiments, effects of the in-plane electric field on the g -factors and Sentaurus TCAD simulations.
 - ²⁷ L. M. Roth, *Phys. Rev.* **118**, 1534 (1960).
 - ²⁸ R. Hanson, L. P. Kouwenhoven, J. R. Petta, S. Tarucha, and L. M. K. Vandersypen, *Rev. Mod. Phys.* **79**, 1217 (2007).
 - ²⁹ I. A. Merkulov, A. L. Efros, and M. Rosen, *Phys. Rev. B* **65**, 205309 (2002).
 - ³⁰ An experimental work has appeared (*Nat. Commun.* **4**, 1768 (2018)) subsequent to our submission, that measures the difference in g -factors between two neighboring QDs in a Si/SiO₂ sample for different directions of B_{ext} . Their findings validate our prediction. The authors also observe a further reduction in the g -factor difference for B_{ext} along [001] direction, due to the suppression of both the Rashba and Dresselhaus SOI along [001], while for [100] only the Dresselhaus SOI gets suppressed. However, we need at least some tunability of the g -factor ($\frac{dg}{dF_z}$) to selectively address the qubits, which is possible through the weaker Rashba SOI along [100] but might not be possible along [001].

ACKNOWLEDGMENT

This work was supported by the U.S. Army Research Office (W911NF-13-1-0024, W911NF-12-0607), the Australian Research Council (CE11E0001017), and the NSW Node of Australian National Fabrication Facility. Computational resources on nanoHUB.org, funded by the

NSF grant EEC-0228390, were used.